



Available online at www.sciencedirect.com



ScienceDirect

Reliability Engineering and System Safety 00 (2014) 1–21

Reliability
Engineer-
ing &
System
Safety

Coupling mode-destination accessibility with a quantitative seismic-risk assessment to identify at-risk communities

Mahalia Miller^a, Jack W. Baker^a

^aStanford University, Stanford, CA USA

Abstract

In this paper, we develop a framework for coupling mode-destination accessibility with a quantitative seismic-risk assessment to identify communities at a high risk for travel disruptions after an earthquake. Mode-destination accessibility measures the ability of people to reach destinations they desire; it is calculated as the log value of the sum of a function of the utilities of each destination over all possible destinations and travel modes, where the utility decreases if getting to that destination is more costly or time-intensive. We use a probabilistic seismic risk assessment procedure, including a stochastic set of earthquake events, ground-motion intensity maps, damage maps, and realizations of traffic and accessibility impacts. For a case study of the San Francisco Bay Area, we couple our seismic risk framework with a practical activity-based traffic model. As a result, we quantify accessibility risk probabilistically by community and household type. We find that accessibility varies more strongly from location to location than between income classes, and we identify particularly at-risk communities. We also observe that communities more conducive to local trips by foot or bike are predicted to be less impacted by losses in accessibility.

© 2014 Published by Elsevier Ltd.

Keywords: Infrastructure, Risk, Earthquakes

1. Introduction

Seismic risk assessment in earthquake engineering tends to focus on buildings, bridges, and the performance of infrastructure systems. For measuring the performance of transportation systems, researchers typically use engineering-based metrics such as the post-earthquake connectivity loss, which quantifies the decrease in the number of origins or generators connected to a destination node [e.g., 1], or the post-earthquake travel distance between two locations of interest [e.g., 2]. These frameworks have provided insight into seismic vulnerability and possible risk mitigation. However, the link to the human ramifications can be limited.

In the field of vulnerability sciences, researchers have long stressed the importance of the impact on human welfare from earthquakes. For example, Bolin and Stanford write that, “‘Natural’ disasters have more to do with the social, political, and economic aspects than they do with the environmental hazards that trigger them. Disasters occur at the interface of vulnerable people and hazardous environments” [3]. A recent World Bank and United Nations report echoed this idea that the effects on human welfare turn natural hazards into disasters [4].

Historical events emphasize the complex social effects of earthquakes. For example, on one hand the 1994 Northridge earthquake caused major damage to nine bridges, which, while significant, represented only 0.5% of the bridges estimated by Caltrans to have experienced significant shaking [5]. On the other hand, over half of businesses reported closing after the earthquake with 56% citing the “inability of employees to get to work” as a reason [6]. Furthermore, the total economic cost of transport-related interruptions (“commuting, inhibited customer access, and

18 shipping and supply disruptions") from this earthquake is estimated at 2.16 billion USD (2014) [7], using the consumer price index to account for inflation.

20 An emergent trend in earthquake engineering is estimating the cumulative extra time needed for travel after a
 21 simulated future earthquake, sometimes called travel time delay [e.g., 8, 9]. This performance measure captures basic
 22 re-routing due to road closures and enables identifying roads more likely to be very congested. Travel time approx-
 23 imately measures one aspect of the impact on people, but does not capture the fact that some destinations and trips
 24 have higher value than others. Furthermore, this approach measures the impacts by focusing on aggregate regional
 25 effects rather than individual communities and demographic groups. Some recent work has looked at other metrics,
 26 such as the qualitative criteria-based metric "disruption index" [10]. However, this does not provide a quantitative link
 27 between the technical impact and the human ramifications. Other work has looked at resiliency, but defined it in pure
 28 engineering terms, such as percentage of a simplified road network that is functional [11]. Outside of transportation
 29 systems, some researchers have investigated the interplay between earthquake damage, such as damage to the electric
 30 power and wastewater networks, and the usability of houses and other buildings; this represents an important first
 31 step [12].

32 In contrast to the work on transportation-related seismic risk, urban planning has a long tradition of studying the
 33 impact on people of events and policy [13]. Accessibility is one metric popular in urban planning to measure the
 34 impact of different transportation network scenarios, and it measures how easily people can get to desirable destina-
 35 tions, which is one measure of social impact [14]. Within urban planning, accessibility has been measured in many
 36 ways, including individual accessibility, economic benefits of accessibility, and mode-destination accessibility [15].
 37 The mode-destination accessibility is computed by taking the log value of the sum of a function of the utilities of each
 38 destination over all possible destinations and travel modes, where the utility decreases if getting to that destination is
 39 more costly or time-intensive [16]. This choice of accessibility definition is particularly applicable to quantifying the
 40 impacts of catastrophes, such as earthquakes, because certain destinations might be more critical for people in certain
 41 locations or from different socio-economic groups (such as low income or high income). However, this accessibility
 42 measure has not yet been linked to risk assessment. In addition, the majority of work to date assumes that travel
 43 demand and mode choice will remain unchanged after a future earthquake, which historical data suggests is not the
 44 case [7]. A first step towards considering variable demand is work in the literature that varies demand by applying a
 45 constant multiplicative factor on all pre-earthquake travel demand [8].

46 In this paper, we develop a framework for coupling mode-destination accessibility with a quantitative seismic-risk
 47 assessment to identify at-risk populations and measure the accompanying impacts on human welfare. We illustrate our
 48 approach with a case study of the San Francisco Bay Area transportation network, including highways, local roads,
 49 and public transportation lines. This study analyzes a set of forty hazard-consistent earthquake scenarios, ground-
 50 motion intensity maps, and damage maps, as introduced in [17] using the optimization procedure proposed in [18].
 51 For each of these damage maps, we model damage with a practical, agent-based transportation model used by the
 52 local transportation authorities that includes damage to bridges, roads, and transit lines, and varies demand. Then,
 53 with this model, we estimate the predicted losses in accessibility according to 12 socio-economic groups used by local
 54 planners for the case study region, based on income class and the ratio of personal vehicles to workers in a household.

55 2. Case study: San Francisco Bay Area

56 2.1. Case study overview

57 We focus on the San Francisco Bay Area, a seismically-active region, to illustrate our approach (Figure 1). The
 58 area follows a polycentric metropolitan form, with San Francisco as the primary center and other jobs concentrated
 59 in suburban centers, such as Silicon Valley [19]. The region has a wide array of trip patterns for mandatory and
 60 non-mandatory trips. Furthermore, trip times and routes vary greatly depending on travel preferences and workplace
 61 locations [19]. Thus, we might expect noticeable disparities between households in the risk of travel time delays due
 62 to earthquakes.

63 This analysis considers the complex web of roads and transit networks of the case study area. The roads are
 64 modeled by a directed graph $G = (V, E)$, where V is a finite set of vertices representing intersections, and the set E ,
 65 whose elements are edges representing road links, is a binary relation on V . In this model, $(|V|, |E|) = (11,921, 32,858)$
 66 including centroidal links and $(|V|, |E|) = (9,635, 24,404)$ without. Centroidal links do not correspond to particular

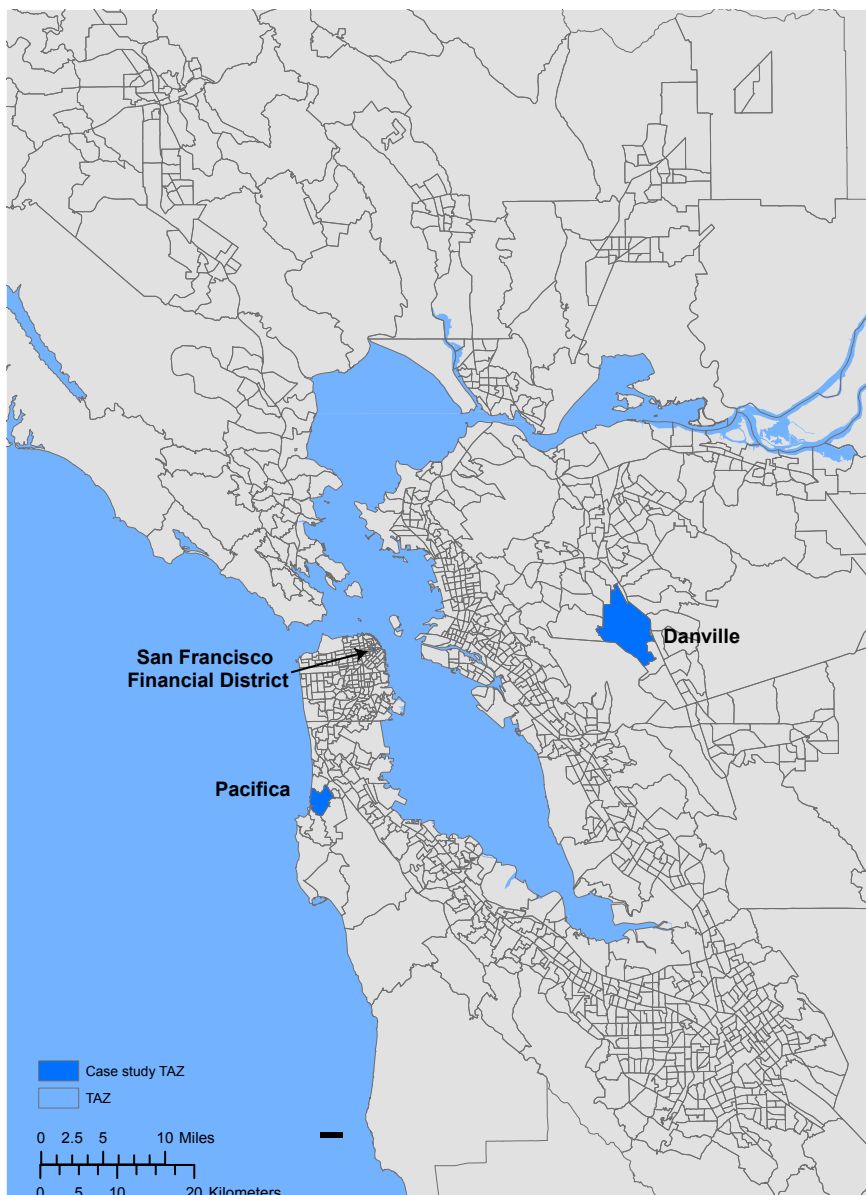


Figure 1. Study area: San Francisco Bay Area, CA with specific travel analysis zones (TAZs) used in the case study marked in blue.

physical roads but instead capture more subtle travel flows, such as from outside the study area or the flow of people to and from some minor local roads. We also in 43 transit networks, as detailed in [17].

We model damage from ground shaking intensity to a set of 1743 highway bridges impacting the road and some transit networks, with data provided by the California Department of Transportation (Caltrans), and 1409 structures impacting the rapid transit network, BART, with data provided by that agency. We refer readers to [17] for more details about matching these structures, hereafter called components, to the relevant road and transit networks.

2.2. Ground-motion intensity maps

2.2.1. Theory

We now describe how to produce a set of maps with ground-motion intensity realizations at each location of interest, and corresponding occurrence rates that reasonably capture the joint distribution of the ground-motion intensity. First, we generate Q earthquake scenarios from a seismic source model. The seismic source model specifies the rates at which earthquakes of specified magnitudes, locations, and faulting types will occur. This set of earthquake scenarios is comparable to a stochastic event catalogue in the insurance industry.

Second, for each earthquake scenario in the seismic source model, we use an empirical ground-motion prediction equation (GMPE) [e.g., 20] to model Y , the resulting intensity measure at each location of interest.

Then, for each of the Q earthquake scenarios, we sample b realizations of the spatially-correlated ground-motion intensity residual terms [e.g., 26]. Once residuals are sampled, the total log ground-motion intensity (Y) is computed as

$$\ln Y_{ij} = \overline{\ln Y(M_j, R_{ij}, V_{s30,i}, \dots)} + \sigma_{ij}\epsilon_{ij} + \tau_j\eta_j \quad (1)$$

where j is the ground-motion intensity map index ($j = 1, \dots, m$ where $m = Q \times b$), ϵ_{ij} is the normalized within-event residual in $\ln Y$ representing location-to-location variability and η_j is the normalized between-event residual in $\ln Y$ and the other parameters are defined above. Both ϵ_{ij} and η_j are normal random variables with zero mean and unit standard deviation. The vector of ϵ_{ij} can be modeled by a spatially-correlated multivariate normal distribution [e.g., 27] and the η_j by a standard univariate normal distribution.

The result is a set of m ground-motion intensity maps (e.g., Figure 2(a)). Since we simulate an equal number (b) of ground-motion intensity maps per earthquake scenario, the annual rate of occurrence for the j^{th} ground-motion intensity map is the original rate of occurrence of the earthquake scenario, divided by b . We denote the rate associated with the j^{th} ground-motion intensity map as w_j .

2.2.2. Implementation

To generate a stochastic catalog of ground-motion intensity maps, we use the OpenSHA Event Set Calculator [28]. This software outputs the mean, $\ln Y_{ij}$, and standard deviation values, σ_{ij} and τ_j , for all locations of interest for a specified seismic source model and ground-motion prediction equation, which are needed inputs for Equation 1. The intensity measure is the 5%-damped pseudo absolute spectral acceleration (Sa) at a period $T = 1s$, which is the required input to the fragility functions below. This spectral acceleration value represents the maximum acceleration over time that a linear oscillator with 5% damping and a period of 1 second will experience from a given ground motion. We calculate these values at each component location (bridges and other structures). Using one ground-motion intensity measure per component is a common simplification of the time-varying acceleration dynamics [e.g., 29, 9] that may have lower errors for components with a natural period near 1 second as opposed to long-span bridges. We use the UCERF2 seismic source model [30], Wald and Allen topographic slope model for the shear wave velocity $V_{s30,i}$ [31], and the Boore and Atkinson [20] ground-motion prediction equation. We simulate the ground-motion intensity maps by combining the mean terms from the Event Set Calculator and spatially-correlated residual terms of the ground-motion intensity (using [27]) according to the basic ground-motion model (eq. 1).

2.3. Damage maps

2.3.1. Theory

Calculating network performance risk requires assessing the structural damage of relevant components after future earthquakes. The link between ground-motion intensity and structural damage is often provided by *fragility functions*. Fragility functions express $P(DS_i \geq ds_\zeta | Y_{ij} = y)$. We assume one component, such as a bridge, per site location, so we

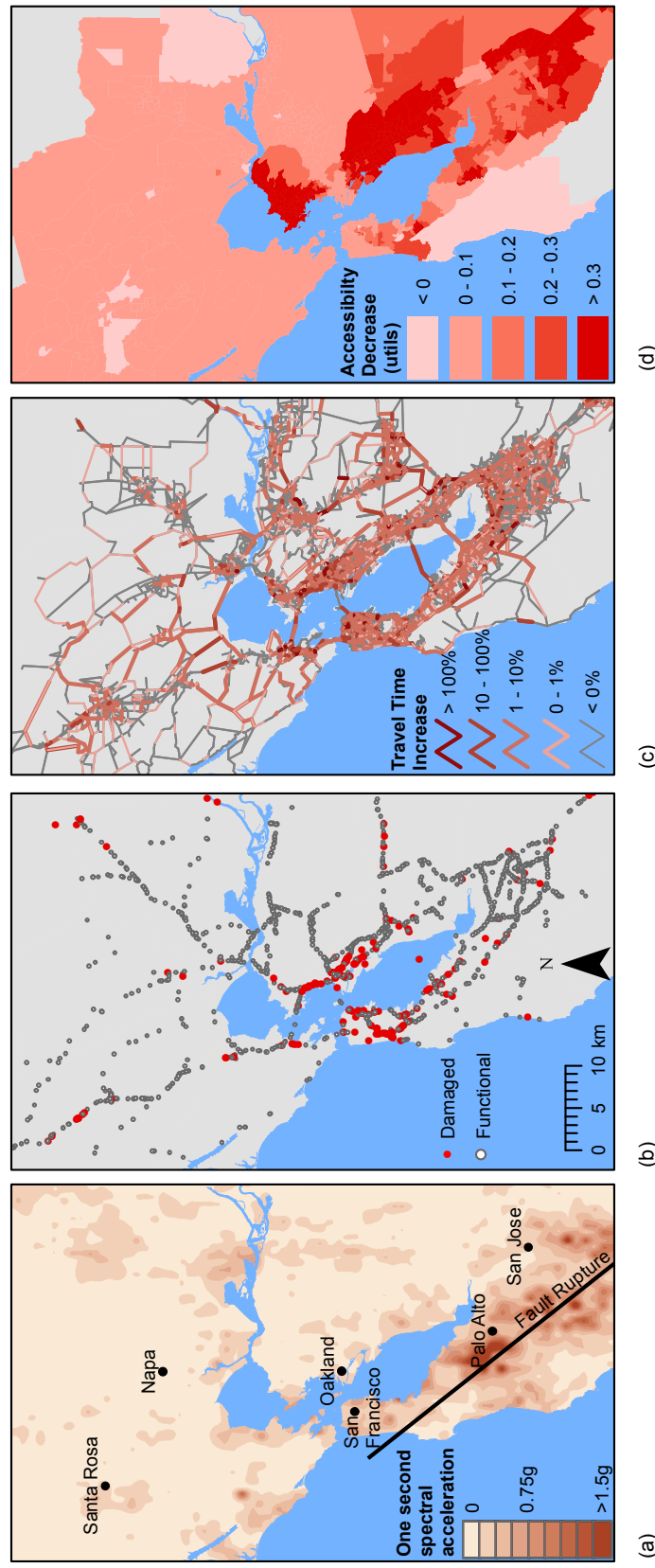


Figure 2. Illustration of the risk framework for one earthquake event including a) One-second spectral acceleration (ground-motion intensity) map with earthquake rupture, b) bridge (component) damage map, c) map of travel time increase (network-performance measure) values, and d) map of accessibility values averaged over all market segments by travel analysis zone (TAZ).

113 will identify both components and site locations via the index i . Using that notation, DS_i is a discrete random variable
 114 whose value represents the damage state for the i^{th} component and ds is a damage state threshold of interest. The
 115 damage state is conditioned on a realization, y , of the random variable Y_{ij} , the ground-motion intensity at the i^{th} site
 116 and j^{th} ground-motion intensity map. Researchers have calibrated fragility functions using historical post-earthquake
 117 data [e.g., 32], experimental and analytical results [e.g., 33], hybrid approaches, and expert opinion. Other work has
 118 investigated correlated damage states [e.g., 34].

119 By sampling a damage state for each component, with probabilities obtained from the fragility functions given
 120 the ground-motion intensity, we produce a damage map (e.g., Figure 2(b)). The damage map has a realization of the
 121 damage state of each relevant component. This sampling process can be repeated multiple times to simulate multiple
 122 damage maps per ground-motion intensity map. For example, if equal numbers of damage maps are sampled per
 123 ground-motion intensity map (c damage maps per ground-motion intensity map), the weight of the j^{th} damage map
 124 should be adjusted accordingly to w_j , where $w_j = \frac{w_j}{c}$, and $j' = 1, \dots, J$.

125 *Functional percentage* relationships link the component damage to the functionality of network elements. For
 126 example, in a road network, when a bridge collapses, the traffic flow capacity of the road it carries and it crosses
 127 can be modeled as reduced to zero. These relationships are typically derived from a combination of observation
 128 and expert opinion, often due to data scarcity [35]. Furthermore, the relationships are typically deterministic for a
 129 certain component damage state and restoration time [35]. Thus, in this paper, each damage map corresponds to a
 130 functionality state for every element of the network.

131 2.3.2. Implementation

132 *Component damage.* For the case study, we use fragility functions of the following form to provide the link between
 133 ground-motion shaking and component damage:

$$P(DS_i \geq ds_\zeta | Y_{ij} = y) = \Phi\left(\frac{\ln y - \lambda_{\zeta,i}}{\xi_{\zeta,i}}\right), \quad (2)$$

134 where Φ is the standard normal cumulative distribution function, $\lambda_{\zeta,i}$ and $\xi_{\zeta,i}$ are respectively the mean and standard
 135 deviation of the $\ln Y_{ij}$ value necessary to cause the ζ^{th} damage state to occur or be exceeded for the i^{th} component,
 136 and the other variables are defined above. By using the previous equation and the inverse method, we can sample
 137 realizations of component damage states for a given ground-motion intensity.

138 The California Department of Transportation (Caltrans) provided the fragility function values $\lambda_{\zeta,i}$ and $\xi_{\zeta,i}$ used
 139 in this study for the highway components in summer 2012, which was last updated in 2007 and includes various
 140 retrofitted bridges [36]. The $\lambda_{\zeta,i}$ values are based on component characteristics including number of spans and age
 141 as detailed in [32]. The $\xi_{\zeta,i}$ values are given as a constant. The BART seismic safety group provided the fragility
 142 function values $\lambda_{\zeta,i}$ and $\xi_{\zeta,i}$ used in this study for the BART-related components for the state of the network in summer
 143 2012. Data is available for the aerial structures, primarily in the East Bay, but not tunnels. The BART fragility
 144 function values correspond to the safety performance goals under the recent retrofit program [37]. The numbers are
 145 comparable to the Caltrans fragility data. For the BART components, however, $\xi_{\zeta,i}$, the standard deviation of the $\ln S_a$
 146 value necessary to cause the extensive damage state to occur or be exceeded, varies depending on the component.
 147 Both sets of fragility functions are based on the assumption that damage can be reasonably accurately estimated by
 148 the ground motion intensity at each site independently, and that the damage state can be reasonably estimated by
 149 an analytical model considering a single ground-motion intensity measure. In addition, the fragility curves do not
 150 directly consider the effects of degradation. Current work is ongoing to refine these assumptions [e.g., 33, 38, 39].

151 Per ground-motion intensity map, we sample one damage map (e.g., Figure 2(b)), which has a realization of the
 152 component damage state at each component location according to the fragility function (eq. 2). The provided fragility
 153 functions do not consider correlation of the structural capacities, but other models could be used [e.g., 34].

154 *Transit network damage.* Each of the 43 transit systems we considered will be impacted differently. For Caltrain,
 155 conversations with managers suggest that given that there is one shared track system, the system would either be
 156 fully operational or not at all. Similarly, managers suggested modeling the VTA system as fully functional or not.
 157 Depending on where the BART train cars are when the earthquake strikes, the agency could accommodate different
 158 emergency plans. However, BART representatives suggested considering that if any part of a route is damaged, the

entire corresponding route would not be operational (but other routes on different tracks might be still operational). In other words, each BART route as well as the Caltrain and VTA routes are each a weakest-link system, so the failure of a single component will cause the route to be non-operational. We modeled the ferry systems as fully functioning for all earthquake events. For all earthquake events including the baseline, trans-bay and cross-county bus lines were discontinued, but main lines in urban areas as well as other local bus networks were maintained per recommendations from the MTC, though they may face delays due to modeled traffic congestion.

Road network damage. The damage state of each component maps directly to the traffic capacity on associated road segments. We use a functional percentage relationship to compute the traffic capacity of relevant road segments. Based on discussions with Caltrans, we consider travel conditions one week after an earthquake, since it is a critical period for decision making. For example, one week after most events, bridges should have been inspected and surface damage should be repaired, but major reconstruction would not have yet begun. According to our functional percentage relationship, at this point in time, the components have one of two classes of functionality, zero traffic capacity and full traffic capacity [35]. We can thus summarize the component damage using two damage states ds_s , $ds_{damaged}$ and $ds_{functional}$, which correspond to the common HAZUS *extensive* or *complete* damage states and the *none*, *slight*, or *moderate* damage states respectively [35]. Thus, the functional percentage relationship assigns zero traffic capacity on road segments that have at least one component in the $ds_{damaged}$ damage state, and full traffic capacity otherwise. We do not consider network damage from sources other than main structural damage from ground shaking, such as tunnel displacement or liquefaction, but the framework allows including such considerations.

2.4. Network performance

2.4.1. Theory

The final step for the event-based risk analysis is to evaluate the network performance measure, X . For this application, we consider a metric popular in urban planning, *mode-destination accessibility change* [e.g., 15, 41, 42] (e.g., Figure 2(d)). Mode-destination accessibility, hereafter referred to as accessibility, measures the distribution of travel destination opportunities weighted by the composite utility of all modes of travel to those destinations, i.e., the ease of someone getting to different destinations weighted by how desirable those destinations are [16, 14]. The utility function for the mode-destination choice may be estimated using a multinomial random utility model where the logsum represents the accessibility value [43, 16, 14]. Namely, accessibility for a particular agent a is

$$Acc_a = \ln \left[\sum_{c \in C_a} \exp(V_{a(c)}) \right], \quad (3)$$

where $V_{a(c)}$ is the utility of the c^{th} choice for the a^{th} person for $a = 1, \dots, A$, and C_a is the choice set for the a^{th} person [16]. Choices refer to travel destinations and the mode of travel (driving, walking, bus, etc.). The units are a dimensionless quantity, *utils*. As an extension, the accessibility values from the previous equation can be converted into equivalent time and dollar amounts using *compensating variation* for cost-benefit studies; for the case study, 0.0134 *utils* (generic measure of utility) equals the value of one minute per day [14, 44, 45] and we conservatively value one hour of time as approximately \$15 [46]. In other words, one *util* is worth approximately \$20 per person per day based on these assumptions. With nearly 7 million people in the region, even small changes in *utils* lead to large economic losses. Since accessibility measures how easily people can get to the destinations they desire, accessibility is used as one of the measures of human welfare [e.g., 14].

Once the accessibility network performance measure is computed for each damage map, we aim to estimate the exceedance rate of different levels of performance. The annual rate, λ , of exceeding some threshold of network performance is estimated by summing the occurrence rates of all damage maps in which the performance measure exceeds the threshold:

$$\lambda_{X \geq x} = \sum_{j'=1}^J w_{j'} \mathbb{I}(X_{j'} \geq x) \quad (4)$$

where x is an accessibility value threshold of interest and $X_{j'}$ is the accessibility value realization for the j'^{th} damage map. The variable $w_{j'}$ is the occurrence rate of the j'^{th} damage map. The indicator function \mathbb{I} evaluates to 1 if the argument, $X_{j'} \geq x$, is true, and 0 otherwise. By evaluating λ at different threshold values, we derive an exceedance curve (e.g., Figure 6).

Income class	Income range, 1989 USD	Income range, 2014 USD
Low	0 - \$25,000	0 - \$47,334
Medium	\$25,000 - \$45,000	\$47,334 - \$85,202
High	\$45,000 - \$75,000	\$85,202 - \$142,004
Very high	more than \$75,000	more than \$142,004

Table 1. Income class definitions for the case study region, as defined by the local planning organization, the MTC [45] and also translated to current 2014 USD using the consumer price index.

203 2.4.2. Implementation

204 We compute accessibility using *Travel Model One* (version 0.3), an activity-based model used by the
 205 Metropolitan Transportation Commission (MTC), the local metropolitan planning organization (MPO) [47]. It represents the full
 206 road network as well as the public transit networks, biking, and walking. Travel demand data consists of the locations
 207 of different households in the case study area, their destination preferences and utilities, their number of vehicles, and
 208 their income and other demographic data [47, 45]. More details can be found in [48]. This data was collected by the
 209 MTC from surveys and census information. We assume that the distributions of travel preferences do not change after
 210 an earthquake, although the actual destinations and trips may vary. For example, if a trip takes a very long time after a
 211 simulated earthquake, it is less likely that a person will choose to take the trip. The result is a *variable* travel demand
 212 model. This model uses a combination of Java code called CT-RAMP [49], and the Citilabs Cube Voyager and Cube
 213 Cluster software programs, which are part of a leading commercial software suite for transportation planning [47].
 214 This model differs from previous representations of this network [e.g., 9, 50], since it includes not only major roads
 215 but also local roads and transit lines. We have provided further details about computing mode-destination accessibility
 216 using this high-fidelity model in [17].

217 This analysis considers 40 interesting and hazard-consistent events, as defined by 40 sets of ground-motion intensity
 218 maps, damage maps, accessibility performance measure realizations, and corresponding annual rates of occurrence.
 219 We selected this set of events with the optimization-based procedure introduced in [18]. Readers are referred
 220 to [17] for more details about this set of events.

221 In the following sections, we first compare region-wide results, and then focus on particular characteristics of
 222 three communities. Finally, we discuss generalizable trends.

223 3. Results and Discussion

224 3.1. Overview of results region-wide

225 In this section, we analyze region-wide trends in accessibility losses for the case study area. We first analyze
 226 each of the 12 socio-economic groups used in practice for the case study region [45]. These socio-economic groups
 227 correspond to all combinations of four income classes (Table 1), and three classes of automobile availability in the
 228 household (zero automobiles, fewer automobiles than household members that work, as many or more automobiles
 229 than household members that work). Each data point for analysis represents a trip by a person of a household from
 230 one of these segments, who is modeled as an agent in the high-fidelity transportation model.

231 General patterns emerge in the expected losses in accessibility. The expected losses are computed by taking
 232 an average of the accessibility results for each of the 1454 travel analysis zones (TAZ) for each earthquake event,
 233 weighted by the adjusted annual likelihood of occurrence from the optimization results.

234 First, we notice that the ratio of cars to the number of people who work in a household is correlated with accessibility
 235 risk; a higher ratio corresponds to higher expected decreases in accessibility. This corresponds to going across a
 236 column in Figure 3. For example, for the first row representing low income households, we notice a marked change in
 237 accessibility across the columns, as indicated by an expanded area of darkened TAZs from left to right (Figure 3(a-c)).
 238 Note that 1 *util* corresponds to a consumer value of compensating variation of approximately \$20 per person per day,
 239 which assumes low (conservative) estimates of the value of time for travel delays and value of getting to destinations.

240 We might expect these households with more cars to take longer trips because there might be a relationship
 241 between needing to travel longer distances and needing an extra car or two in a household. This is indeed the case,
 242 but it is not fully predictive. In fact, there is only a weak trend between average trip length for a TAZ before any

243 earthquake and the predicted impact on accessibility (Figure 4). Instead, we hypothesize that there are other latent
 244 variables correlated with car ownership. For example, the geographic distribution of people without cars varies.
 245 Additionally, in Section 3.5, we will further explore the correlation between the percentage of car-based trips and
 246 accessibility risk. We will show that TAZs with fewer car-based trips tend to have lower risk of accessibility losses.

247 Second, controlling for car ownership, we see a fairly consistent distribution of risk across income class segments.
 248 For example, by looking at households with fewer workers than cars (middle column of Figure 3), the variation from
 249 TAZ to TAZ is significantly more striking than the difference across income segments (Figure 3(b,e,h,k)). Similarly,
 250 while trip lengths are slightly longer for higher income households, the differences are subtle.

251 Thus, for a given TAZ, the differences across incomes are not that great. At the same time though, there is
 252 an unequal geographic distribution of wealth in the San Francisco Bay Area. Because of this, when we aggregate
 253 accessibility risk across TAZs, we see that accessibility risk rises with increasing household income (Figure 6(b)).
 254 Therefore, even though the poor are generally the most vulnerable to natural disasters including hurricanes, floods
 255 and earthquakes, wealthier households in the San Francisco Bay area are more vulnerable than the other income
 256 groups to earthquake-related accessibility risk.

257 Next, we consider which geographic parts of the San Francisco Bay Area are at an elevated risk. The results show
 258 regions of high risk: in the East Bay due East of San Francisco, in the suburbs of San Jose, along the coastal and
 259 Bay-side regions South of San Francisco (Millbrae and Pacifica, e.g.), and in parts of San Francisco (South-Central
 260 neighborhoods including Westland Highlands and Glen Park neighborhoods). One may have expected more high risk
 261 areas on the San Francisco Peninsula, because of the San Andreas fault, which can generate large magnitude events.
 262 In contrast, the East Bay has higher shaking levels at more moderate return periods, due to the higher relative annual
 263 frequency of events on the Hayward Fault; this is correlated to bridge damage and thus road closures. Furthermore,
 264 the data suggests that both the more common moderate-magnitude East Bay events and the rare higher-magnitude
 265 San Andreas events can cause accessibility problems for the East Bay. Figure 5 shows one sample realization of a
 266 M6.85 Hayward event and one sample realization of a M7.45 San Andreas event—both follow the general trend of
 267 high predicted accessibility losses in the East Bay. In contrast, while any events could contribute to the risk in San
 268 Francisco, our model results show the main accessibility losses in San Francisco corresponding to the San Andreas
 269 events. Figures 5(c,d) provide one such example. Figures 5(e,f) show an example of a lower magnitude event farther
 270 away from the main population centers, a M6.35 event in the Great Valley Pittsburg-Kirby Hills Fault. This shows
 271 how the range of more minor faults in the East Bay can contribute to that area's risk. Also, we have shown the results
 272 for one socio-economic group in Figure 5, but the other socio-economic groups follow the same general patterns,
 273 albeit with different specific values.

274 Finally, we can examine the rates of loss exceedance (eq. 4). Figure 6 shows a similar shape to the loss exceedance
 275 curves for other metrics such as portfolio losses and travel time delay [17]. Note that the results are primarily valid
 276 in the 100 to 2475 year return periods, since this is the range chosen for the map selection optimization problem.
 277 Recognizing that the impact varies significantly by TAZ, as indicated by Figure 3, we also examine the accessibility
 278 loss exceedance curve for three communities: part of the San Francisco financial district, Danville, and Pacifica
 279 (Figure 1). These correspond to TAZ IDs 2, 1161, and 224 respectively. This part of the San Francisco financial
 280 district represents an area with relatively low expected changes in accessibility (Figure 3), whereas Danville and
 281 Pacifica are at an elevated risk in almost all socio-economic groups (Figure 3). The general trends are corroborated by
 282 the loss exceedance curves for these three communities (Figure 6(a) shows an example for the socio-economic group
 283 with medium income households with fewer cars than workers). In other words, the average middle-class person from
 284 Danville in a household with fewer cars than people who work is expected to experience travel-related losses up to 1
 285 *utils* per day after a rare earthquake, which he or she values at approximately \$20 per day considering a conservative
 286 estimate of travel time and destination value. In contrast, his or her fellow Bay Area resident in San Francisco has
 287 expected losses of only a tenth as much as experienced by a Danville resident. At return periods greater than 100
 288 years, we notice that Danville and Pacifica follow a similar general pattern, which differs dramatically from that of
 289 San Francisco.

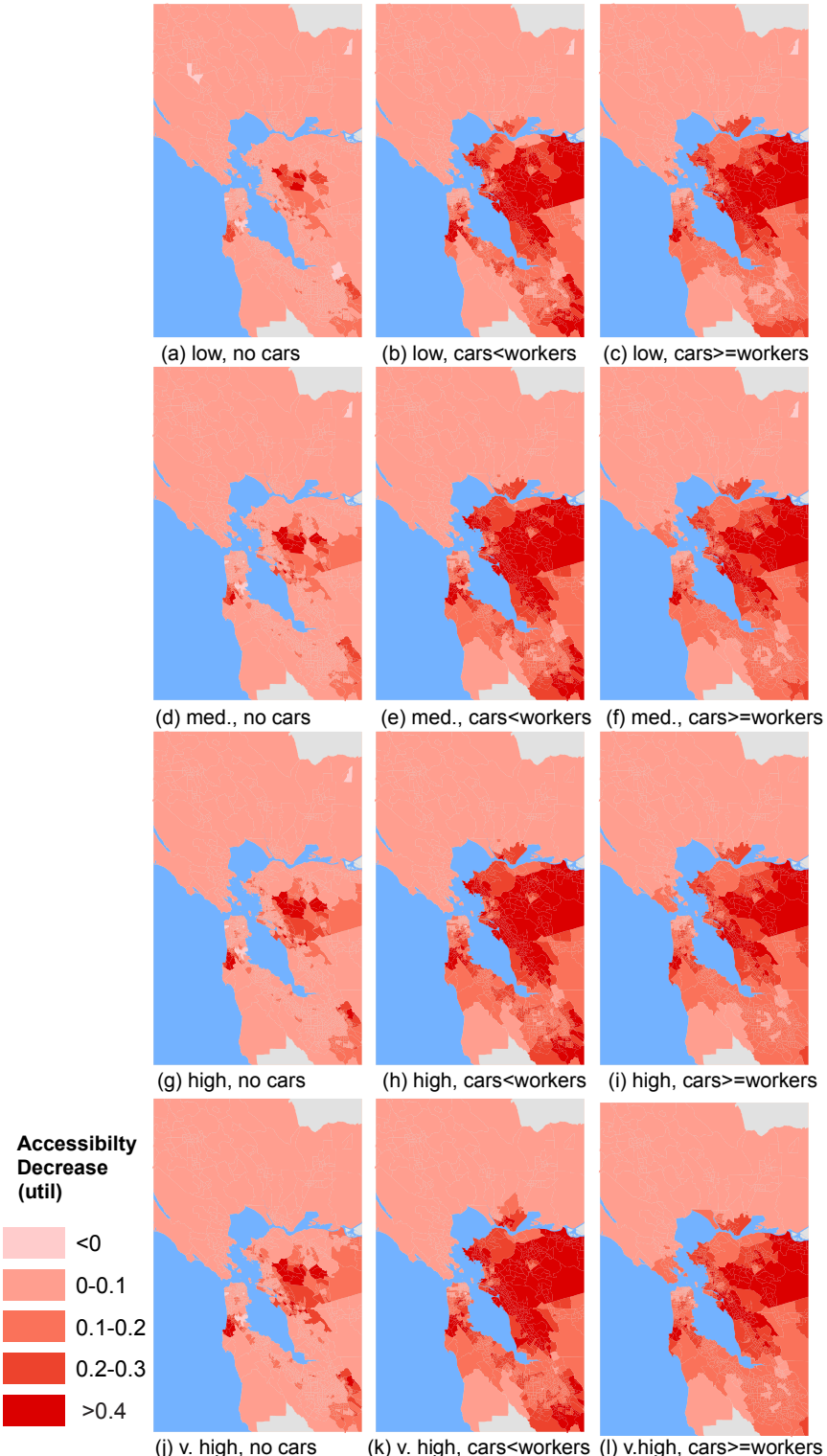


Figure 3. Expected changes in accessibility per person per day for each combination of income class and car ownership group. The darker the color, the greater the losses in accessibility. Low, med., high, and v. high refer to the income class (low, medium, high, and very high respectively). No cars, cars < workers, cars \geq workers refer to the car ownership class (zero automobiles, fewer automobiles than household members that work respectively).

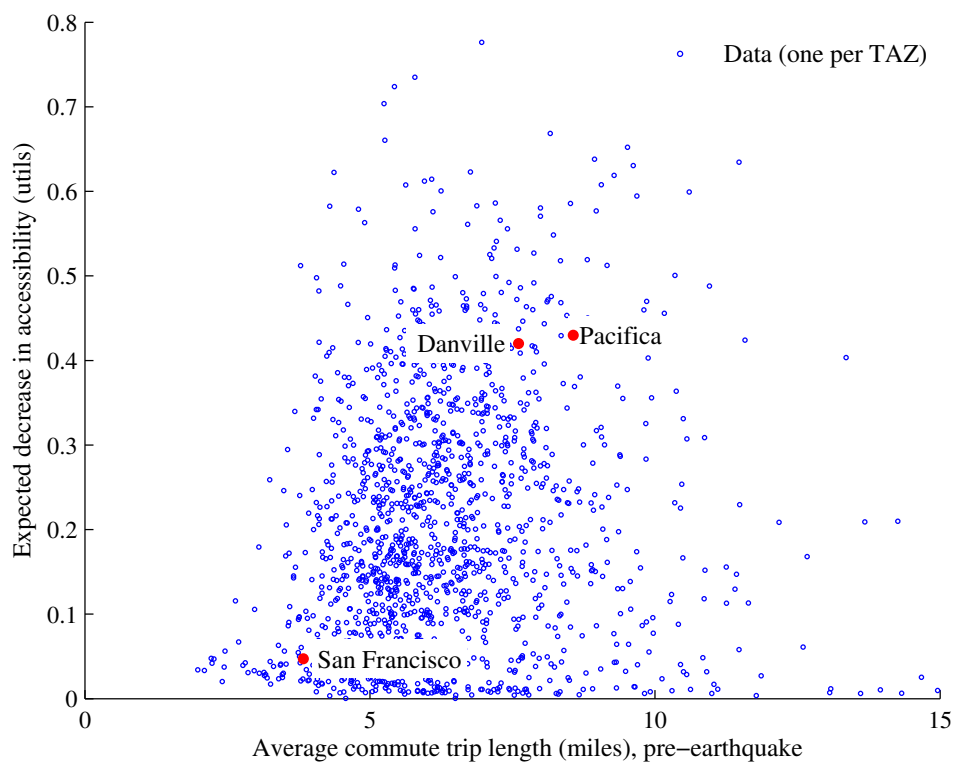


Figure 4. Trip length (pre-earthquake) versus change in total accessibility per person per day. Each dot represents data from one TAZ, and red dots highlight the data points for the three case study communities: San Francisco financial district, Danville, and Pacifica.

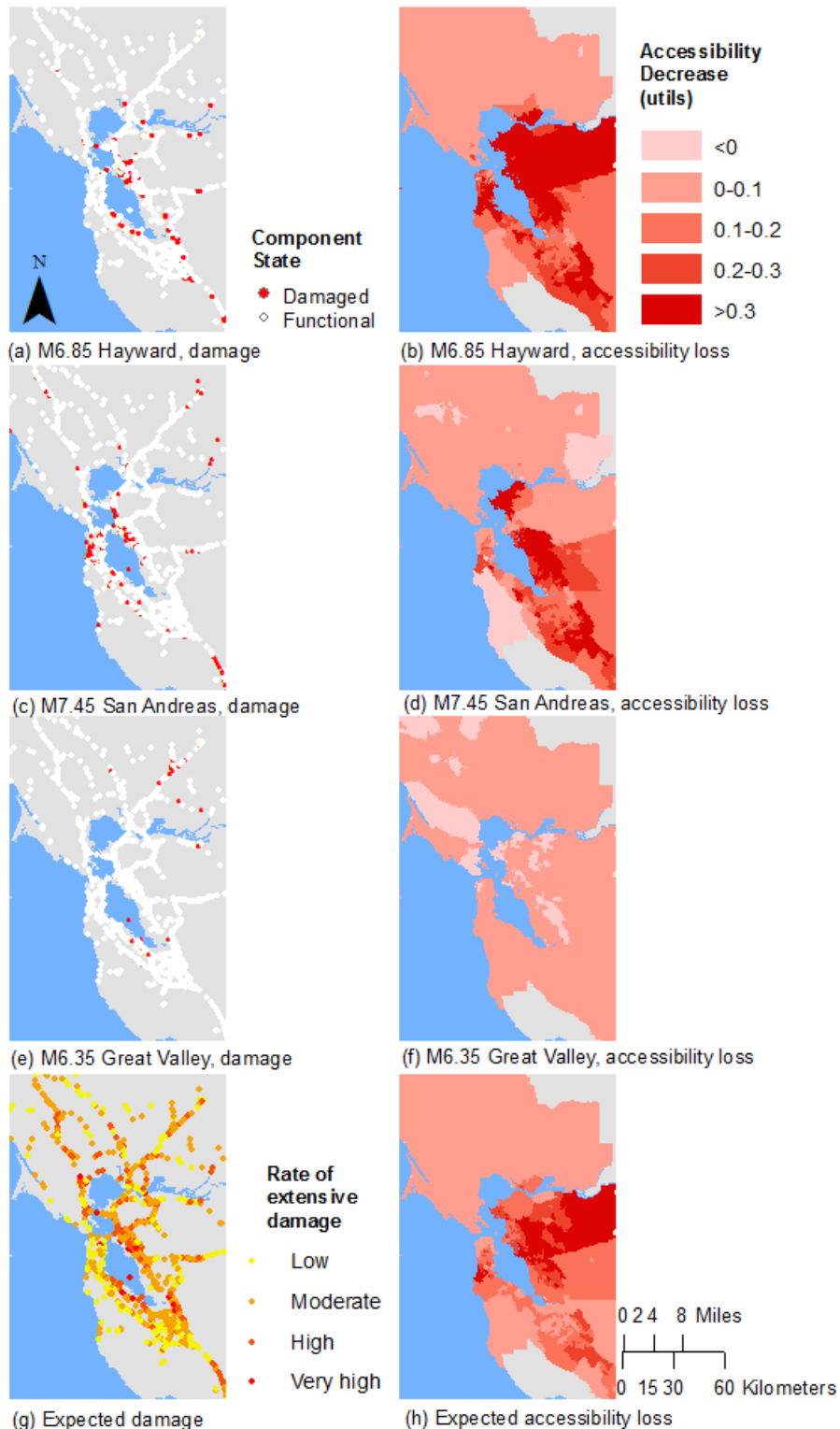


Figure 5. Bridge damage (red = damaged) and corresponding accessibility losses per person per day by TAZ for medium income households with fewer cars than workers. The bottom row has expected values calculated as a weighted average over all events.

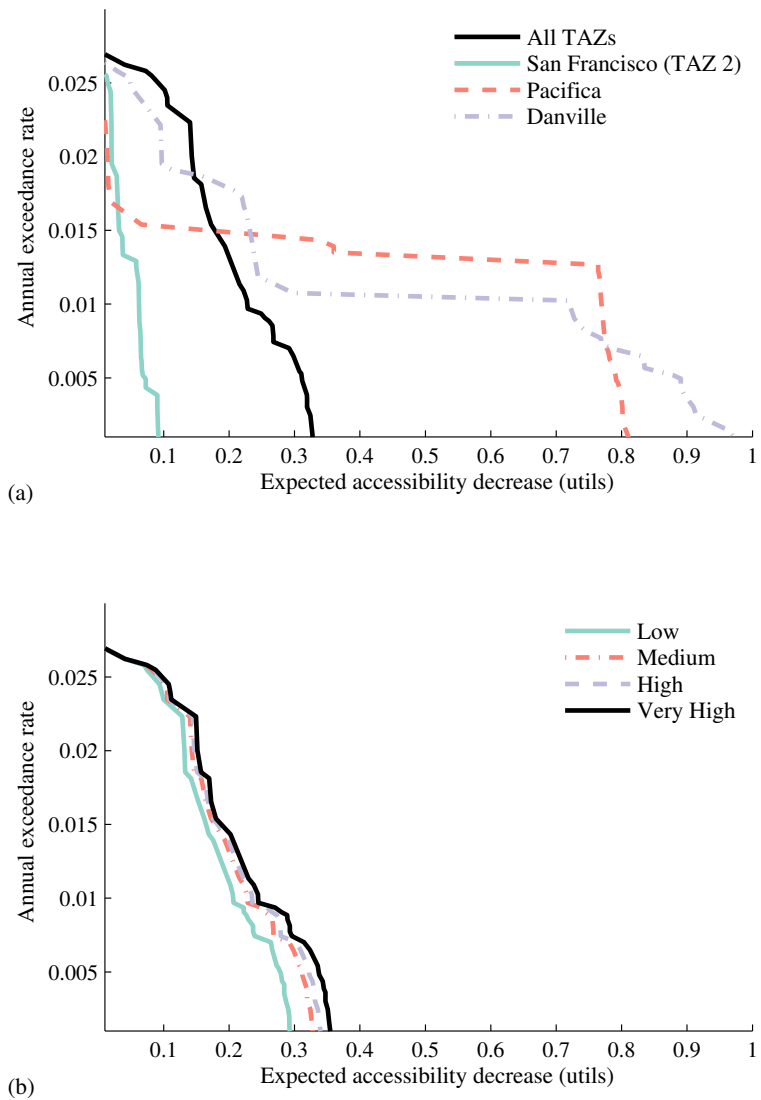


Figure 6. Accessibility annual loss exceedance curve with a comparison by (a) case study TAZs and average over all TAZs and (b) income class; all curves are in *utils* per person per day for medium income households with fewer cars than workers .

290 *3.2. Analysis for San Francisco financial district*

291 In this section, we will explore some possible explanations for why this San Francisco TAZ (Figure 1) has lower
 292 expected accessibility losses than most other communities. First, the financial district of San Francisco differs dramatically
 293 from many other TAZs in that the percentage of trips made by car is relatively small (38% versus an average of
 294 85% across all TAZs). Households traveling by foot or bike will be less influenced by network damage, because the
 295 model considers only damage to the road network and transit systems; thus, foot travel routes and travel times will not
 296 be affected in this model. We also observe that more trips by foot and bike correspond to destinations that are closer
 297 geographically. The impact of travel mode shift post-earthquake will be further explored in Section 3.5.

298 Second, the average time for a trip to and from work is about average for a TAZ in this region and also follows
 299 a similar distribution to that of the other TAZs; the average trip distance for trips is only 7% lower than the average
 300 for all trips region-wide. Since the trip time and length are relatively typical, but the accessibility is much lower than
 301 average, the trip time and length do not explain the differences in accessibility losses.

302 In summary, the data suggests that a major cause for the low expected accessibility impact for the financial
 303 district of San Francisco is the lower relative dependence on cars for mobility. In the next section, we will contrast
 304 the San Francisco example with results from Pacifica, another Peninsula community that, nonetheless, is expected to
 305 be at high risk of losses in accessibility.

306 *3.3. Analysis for Pacifica*

307 We might not suspect that Pacifica would be at an extremely elevated risk of accessibility losses across most
 308 market segments, as compared to other communities very close to earthquake faults. For example, the percentage of
 309 pre-earthquake car-based trips is around average for the case study area (88% versus an average of 85%). In contrast
 310 to most other regions, however, Pacifica is wedged between the Pacific Ocean to the West and the coastal mountains to
 311 the East. Indeed, the main access road is California Highway 1, which has various vulnerable bridges included in the
 312 case study dataset. There are no viable alternative routes on local roads. Since almost all trips are by car from Pacifica
 313 and the average trip length is much longer than the region-wide average (108% longer), the road issue is particularly
 314 serious.

315 As a comparison, consider the next main town along the Pacific coast, Half Moon Bay, about 13 miles South. Half
 316 Moon Bay has significantly lower expected accessibility losses compared to Pacifica (0.11 *utils* per day for a person
 317 in Half Moon Bay in middle income household with fewer cars than workers, given an event in the dataset, versus
 318 0.43 *utils* per day for a similar person in Pacifica). While the seismic hazard is similar, the population is about one
 319 third the size, so there is less demand for the limited road capacity [51]. Furthermore, and likely most significantly,
 320 Half Moon Bay has a key alternative to California Highway 1, California Highway 92, which links to Silicon Valley
 321 and the main highways of that region (US-101 and I-280). Our results indicate that since Pacifica is unusually reliant
 322 on one road with key vulnerabilities for access, it has an elevated risk for losses in accessibility.

323 *3.4. Analysis for Danville*

324 We will first examine the trip length characteristics for Danville. The distribution of pre-earthquake commute trips
 325 from Danville is shifted towards both longer distance and longer time than the communities we have studied so far;
 326 for example, the average length of a trip from Danville is 85% longer than the average over all trips originating from
 327 any TAZ. More specifically, there is a relatively higher proportion of trips taking 60–74 minutes and traveling over 40
 328 miles than in the other communities. The consequence of these longer trips is more opportunities to be impacted by a
 329 road closure, simply because more roads and bridges will be used. Moreover, the road layout near Danville mandates
 330 many highway trips, which increase the likelihood of crossing bridges; bridges are the part of the network for which
 331 we model the vulnerability.

332 Next, we look at patterns of expected bridge damage. Bridge damage is important for many regions, including
 333 Danville, because the percentage of car-based trips is high (85% of all trips on average, and also 85% of Danville-
 334 origin trips). For damage map realizations for the three earthquake events we introduced—M6.85 Hayward Fault,
 335 M7.45 San Andreas Fault, M6.35 Great Valley Fault—some bridges in the Oakland area are in the extensive or
 336 greater damage state (Figure 5(a,c,e)). These correspond to bridge closures in the model. In addition, in the first two
 337 cases, there are closures to the north of Danville, which represents one of the two main travel routes from Danville.
 338 There are also scattered closed bridges to the west of Danville, a top travel corridor for people of Danville because of

Functionality	BART	Caltrain	Muni Light Rail	VTA Light Rail
Full	3	13	25	9
50-99%	10	0	15	0
1-49%	8	0	0	0
None	19	27	0	31

Table 2. Transit network functionality as a count out of the forty simulated events for BART, Caltrain, Muni Light Rail, and VTA Light Rail. Functionality is measured by the percentage of lines that are operational given a damage map (based on a ground-motion intensity map).

the workplace centers in San Francisco, Oakland, and Silicon Valley (all to the west). As for transit, in the first two events, all BART lines are closed, so there are limited alternatives to the popular road routes. The result is that the residents of Danville have reduced access to their normal destinations after all these events.

We can also look at bridge damage in a probabilistic event-set-based manner. The expected damage over all events represents the annual rate of a bridge being in the extensive or complete damage state for an extensively-sampled, hazard-consistent set of damage maps (Figure 5(g)). This figure indicates that bridges in the Oakland-Berkeley area are particularly likely to be damaged. We also see a few high likelihood bridges to the North of Danville. Thus, the data suggests that the relative position of high-risk bridges to Danville contributes to this community's accessibility risk.

3.5. Impact of travel mode shifts and regional variations in travel mode patterns

First, we compare patterns of transit system damage with patterns of travel mode shifts after earthquake events. Over all the simulated events, taking a weighted average by the annual likelihood of each event, we see a reduction in transit ridership (25% weighted average decrease from the base case). This is not surprising. The heavy rail systems (BART and Caltrain) are not fully operational in most of the forty simulated events (Table 2), and these have heavy ridership. The light rail systems (VTA and Muni light rail) also suffered losses in many events (Table 2). The result is an average increase in the percentage of trips by the other modes (foot, car, and bike).

A notable exception is the M6.35 Great Valley, Pittsburg-Kirby Hills Fault earthquake event, as illustrated in Figure 5(e,f). In this event, there were no line closures on the major transit systems (BART, Caltrain, Muni, and VTA Light Rail). There were, however, some bridge closures on the highways (Figure 5(e)). The result was a slight increase in transit ridership and also in trips by foot.

In general, accessibility impact grows with increasing number of damaged transit lines, particularly in combination with high numbers of damaged bridges (Figure 7). The results do not conclusively show that transit is a key contributor to accessibility risk, but based on individual examples, the data suggests this conclusion. For example, in the set of forty events analyzed with the high-fidelity model, the M6.85 Hayward Rogers-Creek and the M7.45 Northern San Andreas Fault event both have a similar number of damaged bridges (around 11%); these are noted by points A and B respectively in Figure 7. These correspond to the bridge damage and accessibility maps in Figures 5(a,b) and 5(c,d) respectively. However, this Hayward Rogers-Creek event has significantly higher accessibility impact. Similarly, the transit impact was different. This Northern San Andreas event had only 4 of the 14 BART lines, all Caltrain, and all VTA Light Rail lines not operational, whereas this Hayward Rogers-Creek event had all 14 of the 14 BART lines, all Caltrain, all VTA Light Rail and 3 of the 8 Muni light rail lines not operational. Thus, the Hayward Rodgers-Creek event featured significantly higher losses to the transit network. Moreover, the differences in accessibility results could not have been predicted from simpler models focusing on bridge portfolio losses, because the percent of damaged bridges was about the same, and the San Andreas event actually corresponded to a greater increase in fixed-demand travel time.

Second, we examine the correlation between a community's walkability, as measured by the percentage of total trips made by that travel mode, and the expected decrease in accessibility by community. We see that an increased percentage of pre-earthquake trips on foot corresponds to a lower average decrease in accessibility (Figure 8). This result corroborates the specific example of the San Francisco Financial District we saw in Section 3.2. Furthermore, on average, the number of by-foot trips slightly increases after the earthquake events where road congestion worsens. This model result is consistent with the observations after the 1995 Kobe earthquake, in which many commuters switched to walking and biking ("non-mechanized modes") in the weeks after the earthquake [7]. In conclusion, the

³⁸⁰ data suggests that TAZs, i.e. communities, which have a greater walkability are also more resilient to earthquake-
³⁸¹ related accessibility risk.

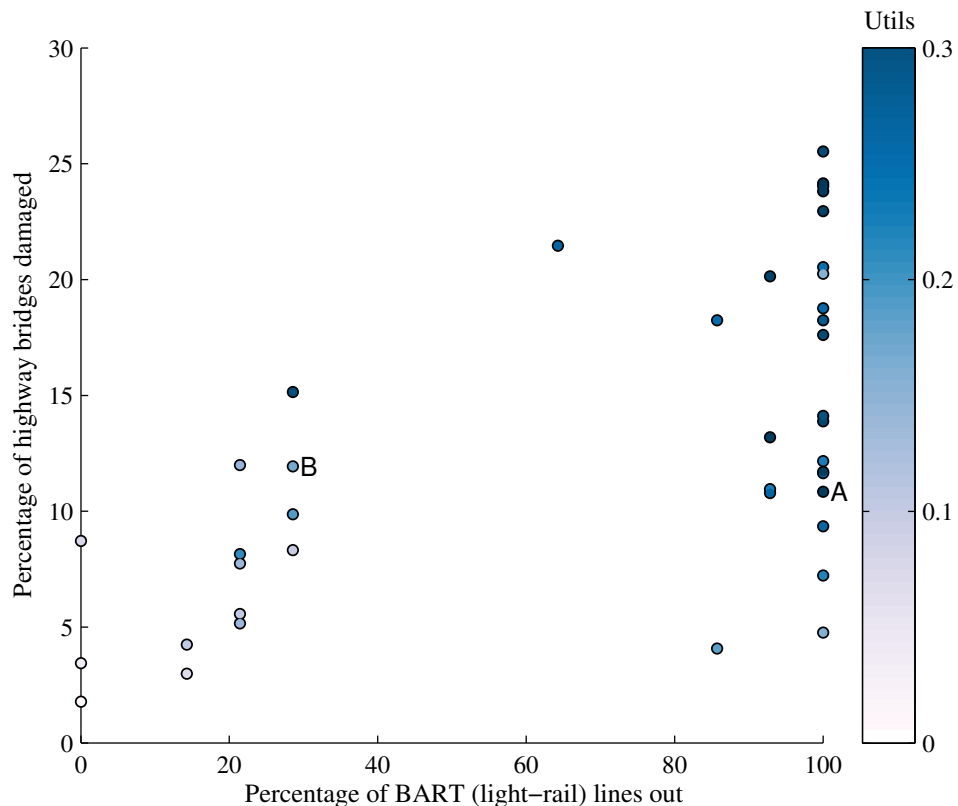


Figure 7. Percentage of BART (heavy-rail) lines not operational versus percentage of highway bridges damaged, where each data point corresponds to one earthquake damage map. The values are color-coded by the average loss in accessibility per day per person over all TAZs for households with the fewer cars than people who work. Two events discussed in this section are marked by the letters A and B.

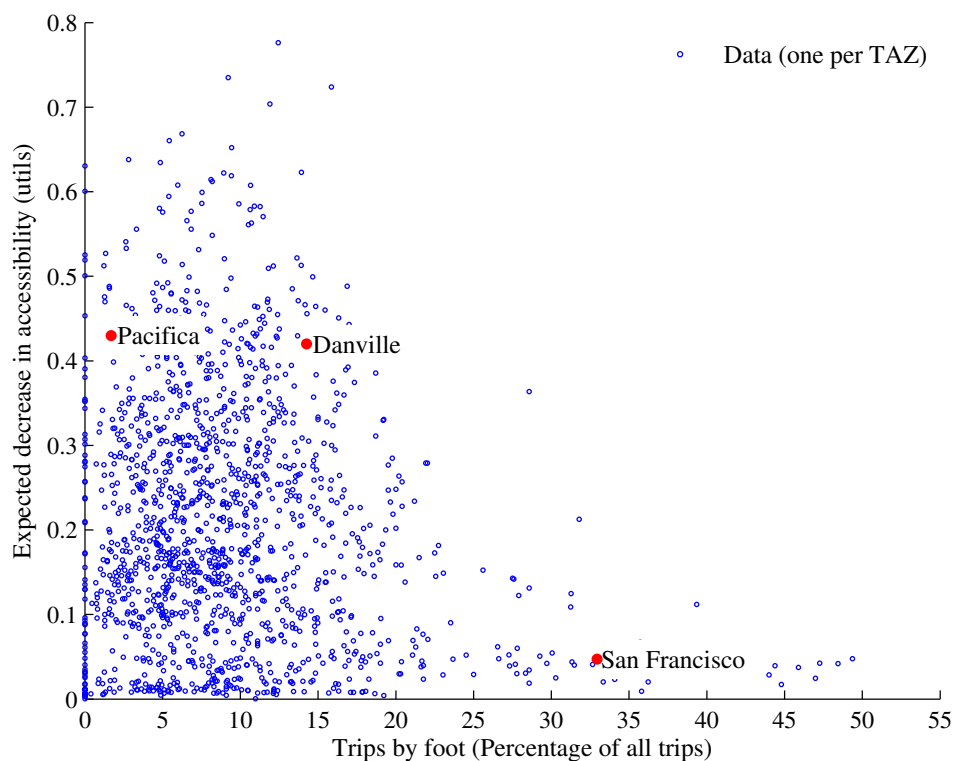


Figure 8. Percentage of total trips by foot (pre-earthquake) versus decrease in total accessibility, measured in *utils* per day (for households with the number of cars less than the number of workers). Each dot represents data from one TAZ, and red dots highlight the data points for the three case study communities: San Francisco financial district, Danville, and Pacifica.

382 **4. Conclusions**

383 Here we have shown how mode-destination accessibility links post-earthquake infrastructure damage to the impact
 384 on human welfare and enables identifying at-risk geographic and demographic groups in a region. Adopting this
 385 state-of-the-art performance metric from the urban planning community, we have illustrated its use for seismic risk
 386 assessment and mitigation through a case study of the San Francisco Bay Area. For the case study, we consider a
 387 set of 40 hazard-consistent earthquake scenarios, ground-motion intensity maps, damage maps, and corresponding
 388 annual rates of occurrence. For each damage map, we processed the data for analysis in a high-fidelity, activity-based
 389 travel model that includes the road network, transit networks, walking and biking options, variable travel demand, and
 390 mode choice. We used this data and model to compute the mode-destination accessibility, a performance measure for
 391 each community and each socio-economic group (defined by income class and car ownership).

392 We saw stark differences in accessibility from location to location. Specifically, we found that areas in the suburbs,
 393 such as the far East Bay, South San Jose and select communities just south of San Francisco, were particularly at risk.
 394 We found that these geographic trends persisted across income classes and car ownership groups. Nonetheless, on
 395 average, higher income households with more cars than workers had the highest risk across the studied socio-economic
 396 groups. One key reason is the geographic clustering of these households in higher-risk areas. Another factor is that
 397 these households tend to take longer daily trips, thus crossing more roads and bridges and possibly increasing the
 398 likelihood of disruption.

399 This study also demonstrated that travel modes shift after an earthquake, and communities who can more easily
 400 adjust are generally predicted to experience lower post-earthquake losses in accessibility. The results suggest that
 401 the walkability of a community, as measured by the percentage of pre-earthquake trips by foot, is closely linked to
 402 reduced accessibility risk. We also found that in almost all of the simulated earthquake events, the transit system,
 403 particularly the heavy rail (BART and Caltrain) lines, is predicted by this model to be severely impacted. The result is
 404 a reduced mode share for transit and increased trips by the other modes (car, walk, and bike). Thus, this study suggests
 405 that not including transit can lead to a nonconservative estimate of seismic risk of transportation systems. The model
 406 shows, however, that when transit is not damaged—which is very rare for this case study—ridership increases.

407 In conclusion, mode-destination accessibility offers important applications for further investigation into the impact
 408 to human welfare of engineering losses and mitigation efforts. This work lays the foundation for future work in risk
 409 mitigation and policy to reduce the vulnerability of at-risk communities. It also suggests that initiatives making
 410 communities more conducive for cycling and walking to work can increase resiliency.

411 **References**

- 412 [1] L. Dueñas-Osorio, J. I. Craig, B. J. Goodno, Seismic response of critical interdependent networks, *Earthquake Engineering & Structural*
 413 *Dynamics* 36 (2) (2007) 285306. doi:10.1002/eqe.626.
- 414 [2] S. E. Chang, M. Shinozuka, J. E. Moore, Probabilistic earthquake scenarios: Extending risk analysis methodologies to spatially distributed
 415 systems, *Earthquake Spectra* 16 (3) (2000) 557–572. doi:10.1193/1.1586127.
- 416 [3] R. C. Bolin, L. Stanford, *The Northridge earthquake: vulnerability and disaster*, Routledge, London; New York, 1998.
- 417 [4] The World Bank and the United Nations, *Natural hazards, unnatural disasters: the economics of effective prevention*, Tech. rep., The World
 418 Bank, Washington D.C. (2010).
- 419 [5] California. Dept. of Transportation. Post Earthquake Investigation Team, *Northridge earthquake, 17 January 1994: PEQIT report*, California
 420 Department of Transportation, Division of Structures, Sacramento, 1994.
- 421 [6] K. J. Tierney, Business Impacts of the Northridge Earthquake, *Journal of Contingencies and Crisis Management* 5 (2) (1997) 87–97.
 422 doi:10.1111/1468-5973.00040.
- 423 [7] P. Gordon, H. W. Richardson, B. Davis, Transport-related impacts of the Northridge earthquake, National Emergency Training Center, 1998.
- 424 [8] A. Kiremidjian, J. Moore, Y. Y. Fan, O. Yazlali, N. Basöz, M. Williams, Seismic risk assessment of transportation network systems, *Journal*
 425 *of Earthquake Engineering* 11 (3) (2007) 371–382. doi:10.1080/13632460701285277.
- 426 [9] N. Jayaram, J. W. Baker, Efficient sampling and data reduction techniques for probabilistic seismic lifeline risk assessment, *Earthquake*
 427 *Engineering & Structural Dynamics* 39 (10) (2010) 1109–1131. doi:10.1002/eqe.988.
- 428 [10] C. S. Oliveira, M. A. Ferreira, F. M. d. S., The concept of a disruption index: application to the overall impact of the July 9, 1998 Faial
 429 earthquake (Azores islands), *Bulletin of Earthquake Engineering* 10 (1) (2012) 7–25. doi:10.1007/s10518-011-9333-8.
- 430 [11] P. Bocchini, D. M. Frangopol, Restoration of bridge networks after an earthquake: Multicriteria intervention optimization, *Earthquake Spectra*
 431 28 (2) (2012) 426–455. doi:10.1193/1.4000019.
- 432 [12] F. Cavalieri, P. Franchin, P. Gehl, B. Khazai, Quantitative assessment of social losses based on physical damage and interaction with infra-
 433 structural systems, *Earthquake Engineering & Structural Dynamics* 41 (11) (2012) 1569–1589. doi:10.1002/eqe.2220.
- 434 [13] F. S. Chapin, *Urban land use planning*, University of Illinois Press, 1970.
- 435 [14] D. A. Niemeier, Accessibility: an evaluation using consumer welfare, *Transportation* 24 (4) (1997) 377396.

- [15] K. T. Geurs, B. van Wee, Accessibility evaluation of land-use and transport strategies: review and research directions, *Journal of Transport Geography* 12 (2) (2004) 127–140. doi:10.1016/j.jtrangeo.2003.10.005.
- [16] S. L. Handy, D. A. Niemeier, Measuring accessibility: an exploration of issues and alternatives, *Environment and Planning A* 29 (7) (1997) 11751194.
- [17] M. Miller, Seismic risk assessment of complex transportation networks, PhD thesis, Stanford University (2014).
- [18] M. Miller, J. Baker, Ground-motion intensity and damage map selection for probabilistic infrastructure network risk assessment using optimization, in review (2014).
- [19] R. Cervero, K.-L. Wu, Polycentrism, commuting, and residential location in the San Francisco Bay area, *Environment and Planning A* 29 (5) (1997) 865–886.
- [20] D. M. Boore, G. M. Atkinson, Ground-motion prediction equations for the average horizontal component of PGA, PGV, and 5%-damped PSA at spectral periods between 0.01 s and 10.0 s, *Earthquake Spectra* 24 (1) (2008) 99–138.
- [21] N. Abrahamson, W. Silva, Summary of the Abrahamson & Silva NGA Ground-Motion Relations, *Earthquake Spectra* 24 (1) (2008) 67–97. doi:10.1193/1.2924360.
- [22] B. Chiou, R. R. Youngs, An NGA model for the average horizontal component of peak ground motion and response spectra, *Earthquake Spectra* 24 (1) (2008) 173–215. doi:10.1193/1.2894832.
- [23] K. W. Campbell, Y. Bozorgnia, NGA ground motion model for the geometric mean horizontal component of PGA, PGV, PGD and 5% damped linear elastic response spectra for periods ranging from 0.01 to 10s, *Earthquake Spectra* 24 (1) (2008) 139–171. doi:10.1193/1.2857546.
- [24] J. W. Baker, C. A. Cornell, Which spectral acceleration are you using?, *Earthquake Spectra* 22 (2) (2006) 293–312. doi:10.1193/1.2191540.
- [25] R. Foulser-Piggott, P. J. Stafford, A predictive model for Arias intensity at multiple sites and consideration of spatial correlations, *Earthquake Engineering & Structural Dynamics* 41 (3) (2012) 431451. doi:10.1002/eqe.1137.
- [26] Y. Han, R. A. Davidson, Probabilistic seismic hazard analysis for spatially distributed infrastructure, *Earthquake Engineering & Structural Dynamics* 41 (15) (2012) 2141–2158. doi:10.1002/eqe.2179.
- [27] N. Jayaram, J. W. Baker, Correlation model for spatially distributed ground-motion intensities, *Earthquake Engineering & Structural Dynamics* 38 (15) (2009) 1687–1708. doi:10.1002/eqe.922.
- [28] E. H. Field, T. H. Jordan, C. A. Cornell, OpenSHA: a developing community-modeling environment for seismic hazard analysis, *Seismological Research Letters* 74 (4) (2003) 406 – 419. doi:10.1785/gssrl.74.4.406.
- [29] M. Shinozuka, Y. Murachi, X. Dong, Y. Zhou, M. J. Orlikowski, Effect of seismic retrofit of bridges on transportation networks, *Earthquake Engineering and Engineering Vibration* 2 (2) (2003) 169–179. doi:10.1007/s11803-003-0001-0.
- [30] E. H. Field, T. E. Dawson, K. R. Felzer, A. D. Frankel, V. Gupta, T. H. Jordan, T. Parsons, M. D. Petersen, R. S. Stein, R. J. Weldon, C. J. Wills, Uniform California Earthquake Rupture Forecast, Version 2 (UCERF 2), *Bulletin of the Seismological Society of America* 99 (4) (2009) 2053–2107. doi:10.1785/0120080049.
- [31] D. J. Wald, T. I. Allen, Topographic slope as a proxy for seismic site conditions and amplification, *Bulletin of the Seismological Society of America* 97 (5) (2007) 1379–1395. doi:10.1785/0120060267.
- [32] N. Basöz, J. Mander, Enhancement of the highway transportation lifeline module in HAZUS, Tech. rep., Final Pre-Publication Draft (#7) prepared for the National Institute of Building Sciences (NIBS) (1999).
- [33] K. N. Ramanathan, Next generation seismic fragility curves for California bridges incorporating the evolution in seismic design philosophy, PhD thesis, Georgia Institute of Technology (2012).
- [34] R. Lee, A. S. Kiremidjian, Uncertainty and correlation for loss assessment of spatially distributed systems, *Earthquake Spectra* 23 (4) (2007) 753–770. doi:10.1193/1.2791001.
- [35] S. Werner, C. Taylor, S. Cho, J. Lavoie, REDARS 2 methodology and software for seismic risk analysis of highway systems (technical manual), Tech. rep., Seismic Systems & Engineering Analysis for MCEER, Oakland, CA (2006).
- [36] Caltrans, Caltrans Seismic Design Criteria Version 1.7, Tech. Rep. SDC 1.7, California Department of Transportation, Sacramento, CA (2013).
- [37] Bechtel/HNTB Team, Design Criteria Volume I, Version 1.2, Tech. rep., San Francisco Bay Area Rapid Transit District, San Francisco Bay Area Rapid Transit District Earthquake Safety Program (2008).
- [38] N. Kurtz, J. Song, P. Gardoni, Time-varying seismic reliability analysis of representative US west coast bridge transportation networks, in: G. Deodatis, B. R. Ellingwood, D. M. Frangopol (Eds.), *Safety, Reliability, Risk and Life-Cycle Performance of Structures and Infrastructures*, CRC Press, 2014, pp. 655–662.
- [39] J. Ghosh, K. Rokneddin, J. E. Padgett, L. Dueas-Osorio, Seismic reliability assessment of aging highway bridge networks with field instrumentation data and correlated failures. I: Methodology, *Earthquake Spectra* 30 (2) (2013) 795–817. doi:10.1193/040512EQS155M.
- [40] S. Pugh, Construction statistics, Tech. rep., California Department of Transportation Division of Engineering Services (2012).
- [41] K. Kockelman, Travel Behavior as Function of Accessibility, Land Use Mixing, and Land Use Balance: Evidence from San Francisco Bay Area, *Transportation Research Record: Journal of the Transportation Research Board* 1607 (-1) (1997) 116–125. doi:10.3141/1607-16.
- [42] P. Waddell, F. Nourzad, Incorporating nonmotorized mode and neighborhood accessibility in an integrated land use and transportation model system, *Transportation Research Record: Journal of the Transportation Research Board* 1805 (-1) (2002) 119–127. doi:10.3141/1805-14.
- [43] C. F. Manski, *Structural analysis of discrete data with econometric applications*, MIT Press, 1981.
- [44] K. A. Small, H. S. Rosen, Applied welfare economics with discrete choice models, *Econometrica* 49 (1) (1981) 105–130. doi:10.2307/1911129.
- [45] D. Ory, Personal communication (2013).
- [46] United States Department of Transportation, Revised departmental guidance: valuation of travel time in economic analysis, US Department of Transportation, Washington, DC.
- [47] G. Erhardt, P. Brinckerhoff, D. Ory, A. Sarvepalli, J. Freedman, J. Hood, B. Stabler, MTC's Travel Model One: applications of an activity-based model in its first year, in: *Innovations in Travel Modeling 2012*, Tampa, Florida, 2012, p. 9.
- [48] P. Waddell, UrbanSim: modeling urban development for land use, transportation, and environmental planning, *Journal of the American Planning Association* 68 (3) (2002) 297–314. doi:10.1080/01944360208976274.

- 501 [49] W. Davidson, P. Vovsha, J. Freedman, R. Donnelly, CT-RAMP family of activity-based models, in: Proceedings of the 33rd Australasian
502 Transport Research Forum (ATRF), Canberra, Australia, 2010, p. 15.
- 503 [50] H. Wakabayashi, H. Kameda, Network performance of highway systems under earthquake effects: a case study of the 1989 Loma Prieta
504 earthquake, in: Proceedings US-Japan Workshop on Earthquake Disaster Prevention for Lifeline Systems, 1992, pp. 215–232.
- 505 [51] U.S. Bureau of the Census, United States Census 2010, Tech. rep., U.S. Census Bureau, Washington D.C. (2010).